ISSN: 0974-8571 Vol.13 No. 1 June, 2021

International Journal of Computational Intelligence in Control

# A convex weighted variational model for selective segmentation: Application to medical images

Afzal Rahman[1*], Haider Ali[1], Noor Badshah[2], Haroon Niaz Ali Khan[1], Muhammad Shabir[3], Shahid Rahman[3] and Khaista Khan[3]

[1]Department of Mathematics, University of Peshawar, Peshawar, 25120, Pakistan, afzal85@uop.edu.pk, haider_uop99@yahoo.com, haroonniaz@uop.edu.pk
[2]Department of Basic Sciences, University of Engineering and Technology Peshawar, Peshawar, 25120, Pakistan, noor2knoor@gmail.com
[3]Department of Computer Sciences, University of Buner, Buner, 19290, Pakistan, shabir_adam@yahoo.com, rahmanshahid059@gmail.com, khaistakhan@gmail.com

*Date of Submission: 15th January 2021 Revised: 27th March 2021 Accepted: 18th June 2021*

*Abstract* - **In medical imaging and many other areas, selective image seg- mentation plays a key role. In this paper, we introduced a unique and novel convex selective segmentation model which contains two stages. The first stage is to achieve a regular approximation associated with the Mumford-shah model to the mark region in the given image. The approximation yields a greater value for the mark region and smaller values for others. In the second stage, we make use of this approximation and implement a thresholding technique to retrieve the object of interest. The approximation can be achieved by the alternating direction method. Experimental results on medical and noisy images are given to testify the importance of the proposed method. The comparisons show that the proposed method works better than other existing methods.**

*Index Terms* _ - Convex, Selective Segmentation, Thresholding technique, Medical Images, Distance function, Alternating Direction Method.

## 1. Introduction

Image segmentation is a major and complicated work in image processing and computer vision. Models based on partial differential equations are famous due to their affability and computational advantage in this field. Variational models can be categorized into two methods namely, region-based methods [1] and edge-based methods [2, 3, 4]. The first and second-order derivatives are used in edge-based techniques. The main defect is the deficiency of robustness in handling noisy images. The popular and effective region- based model is the Mumford-shah (MS) model [1]. The variational problems provoke piecewise smooth solutions with unwrinkled edges. In numerical computation, topological changes are not allowed during the iteration, and parameterizations are necessary. In many applications, such as surgery imitation, medical examination, object tracking, people extract only desired objects from an image. In the aforementioned cases, selective segmentation models are more useful. By using a set of marker points on the contour of significance to the geodesic active contour model Gout *et al.* [5] proposed a geometry constraint. By combining the region term Badshah and Chen [6] made the results better. For images that contain noise, the model became more robust with the region information. To segment the best class of image segmentation issue and taking more complicated features Zhang *et al.* [7] projected an adaptively precise band algorithm. Rada-Chen [8] were used two-level set functions which can perform two tasks simultaneously and pro- posed a new variational model. The first task is to find the segmentation of all edges and the target of the second one is on the selected object that is near to the geometry constraints. Peng *et al.* [9] have proposed an intensity term for 3D liver segmentation. Mabood *et al.* [10] utilized the average image of channels and proposed a selective segmentation model which can extract textural and inhomogeneous objects. Recently C. Liu *et al.* [11] proposed a weighted variational model for selective image segmentation model including weight function to the Mumford-shah model.

To propose a new two-stage weighted convex selective image segmentation model based on the Mumford-Shah model and recently proposed model by C. Liu *et al.* [11] is the central theme of this paper. By using distance and edge detector functions we construct a new weighted function with the impact of different powers of p. In the first step, we chose various marker points around the object of interest. We can find a smooth approximation to the target region, by combining this weighted function into a convex second- order segmentation model. The minimizer of the proposed model must exist, and it will be unique. Many efficient numerical algorithms can be applied by virtue of the convexity of the new model. We demonstrate how to use the alternating direction method to obtain an appropriate numerical algorithm and to show the linear convergence under smooth conditions. In the second step, we make use of this approximation function and perform a thresholding technique to get the object of interest.

This paper is arranged as follows. A brief review of the related segmentation models is given in section 2. In section 3, we demonstrate our model and establish the associated mathematical features. The numerical innovation and its convergence tests are present in section 4. To show the good performance of our approach we present some numerical experiments in section 5. Finally, we draw the consequences of the paper in the last section.

## 2 Related Works

### 1.1 Variational Segmentation Models

For the solution of the curve evolution problems more appropriate method is the level set method [12]. The topological changes are allowed, and the interface is depicted inevitably by the zero-level set of a Lipschitz continuous level set function (LSF). For the implementation of the discretization scheme, the mesh grids should be fixed. Chan and Vese proposed the two-phase MS model [13] for those images which have piecewise constant intensities and the multiphase case [14]. Discontinuous functions are used in piecewise constant level set methods [15, 16, 17] to show distinct phases. Continuous functions should be used in methods of fuzzy membership function [18, 19]. To show the probability of belonging to some specific region these functions ranging from 0 to 1. To overwhelmed local minimum issue of the MS model graph cut method [20] and convex relation methods [21, 22] were proposed. By using a convex variant of the MS model Cai *et al.* [23] proposed a two-stage segmentation model which can be viewed as image segmentation and unification of image restoration. They used the Split-Bregman algorithm [24, 25] and found a unique smooth minimizer and then by thresholding procedure segmented the image. For the purpose to pick the threshold automatically they introduced a K-means method. To propose a new multiphase segmentation model Cai blend image segmentation and image restoration models [26]. In, [27, 28] the methods of Multiatlas segmentation have been projected and showed to be useful. To handle texture characteristics the methods of non- parametric statistical segmentation were proposed in [29, 30]. For video and individuals image segmentations a wavelet method with a shape prior was proposed in [31]. Moreover, about segmentation methods, reader is referring to [32, 33, 34, 35, 36, 37, 38, 39, 40] and the reference therein.

The solution of the following minimization problem is the main objective of the MS model [1]:

$$\left\{\frac{\alpha}{2}\int_{\Omega} |z_0 - z|^2 dx\, dy + \frac{\beta}{2}\int_{\Omega\setminus\Gamma} |\nabla z|^2 dxdy + H^1(\Gamma)\right\}$$

where $H^1$ is the one-dimensional Harsdorff measure. $\alpha, \beta > 0$ and $\Omega \subseteq R^2$ be a connected bounded open set with Lipschitz boundary. $\Gamma$ be a compact curve in $\Omega$ and $f: \Omega \to R$ be a given image. $H^1(\Gamma)$ represents the length of $\Gamma$ for fixed curves. A two-stage variational image segmentation was proposed in [23]. The first step is to obtain a smooth approximation to the original image by solving the underneath convex minimization problem.

$$\left\{\int_{\Omega} |\nabla z| dxdy + \frac{\alpha}{2}\int_{\Omega} |\nabla z|^2 dxdy + \frac{\beta}{2}\int_{\Omega} |z_0 - z|^2 dx\, dy\right\}, \quad (1)$$

where the Sobolov space $W^{1,2}(\Omega) = \{v \in L^2(\Omega)/\partial_j v \in L^2(\Omega), j = 1,2\}$ with

$$L^2(\Omega) = \left\{f(x)/\left(\int_{\Omega} f^2(x)dx\right)^{\frac{1}{2}} < \infty\right\},$$

once $z$ is obtained then in the second stage, by thresholding $z$ properly the segmentation is obtained. The threshold can be provided by the experimenter or obtained automatically by any clustering method, such as convex K-means or K-means methods [41, 42].

### 1.2 Selective Segmentation Models

Selective segmentation that plucks out object of interest from a given image. Like medical diagnosis and security monitoring selective segmentations are important and challenging task. Suppose that $N$ points inside the target are present on the image. Using these marker points $X = \{x_1, x_2, \ldots, x_N\}$, a distance function $d(x): \Omega \to R$ can be defined as [6].

$$d(x) = \prod_{j=1}^{N} \left\{1 - exp^{\left(\frac{-|x - x_j|^2}{2h^2}\right)}\right\}, \qquad x \in \Omega \quad (2)$$

where $h > 0$.

Near the marker points, the distance function is near to zero and far away from the marker points, it approximates to one. Another way to define $d(x)$:

$$d(x) = |x - y| \quad (3)$$

where the edge detection function defined as:

$$\int_{\Gamma} d.gds$$

where $d$ is a distance function.

Badshah and Chen [6] introduced intensity fitting terms like Chan- Vese model [13] and improved the model as: where $\lambda_1, \lambda_2$, and $\beta$ are some constant and use to adjust the regularity and fidelity terms. The boundary between $\Omega_{in}$ and $\Omega_{out}$ is $\Gamma$, constants $c_1$ and $c_2$ are to be optimized. They need to solve the Euler Lagrange Equation of the LSF under the level set formulation. A new adaptive local band level set method was introduced in [7]. Combining the marker and anti-marker set, Nguyen *et al.* [43] proposed a selective segmentation model. Recently Liu *et al.* [44] proposed a new weighted

where $\omega$ is a weight function defined by:

$$\omega^2(x) = 1 - d(x)g(x) \quad (7)$$

They used the method of two stages. In the first stage, they solve a minimization problem based on some marker points and find out a smooth minimizer, and then in the second stage, they use simple thresholds and carried out segmentation.

## 3 The Proposed Weighted Model

In this section, we present our new model and its mathematical analysis. Our methodology contains two steps. In the first step, we solve a minimization problem

where the weight function $\omega$ is to adjust the smoothing and fidelity terms. In this paper, we define the weight function as follows:

$$\omega(x) = \sqrt{1 - d(x)g(x)}, \quad (9)$$

Where $P \geq 2$ and $\omega(x) \in (0,1]$. $d(x)$ distance function and $g(x)$ is an edge detector function and are defined by Eq. (3) and (4) respectively. $g(x)$ is small around the boundaries while $d(x)$ is small around the marker points virtually. The weight function $\omega(x)$ in Eq. (9) is smaller far away from the boundaries and becomes larger near the boundaries because the chosen marker points are near the boundaries. Therefore, we deduce that:

**(1)** Nearby the boundaries, the fidelity term, which is the third term, in Eq. (8), plays an important role, and details have remained.

**(2)** smoothing plays a key role far away from the boundaries. As we can observe from the numerical results complex structures far away from the edges are

$$g(x) = \frac{1}{1 + \beta|\nabla f(x)|^2}$$

The above edge detector function is usually incorporated into segmentation models to use the edge information. An edge-based model was projected as follow in [5]

$$\left\{\beta \int_{\Gamma} d.gds + \lambda_1 \int_{\Omega_{in}} |f - c_1|^2 dxdy + \lambda_2 \int_{\Omega_{out}} |f - c_2|^2 dxdy\right\} \quad (5)$$

variational model for selective image segmentation with application to medical images. They just incorporate a weight function to the Two-stage variational image segmentation model given in Eq. 1. The new model is given as follows:

$$\left\{E(u) := \int_{\Omega} |\nabla u| dxdy + \frac{\alpha}{2}\int_{\Omega} |\nabla u|^2 dxdy + \frac{\beta}{2}\int_{\Omega} \omega^2 |u - f|^2 dxdy\right\}, \quad (6)$$

based on some marker points and find out a smooth minimizer. Then in the second step, we use simple thresholding and carried out segmentation.

### 3.1 Proposed Model

Impressed by the convex model Eq. (1) and the aforementioned selective image segmentation models. We propose the following weighted model with the different impact of $P$:

$$\left\{F(z) := \int_{\Omega} |\nabla z|\, dxdy + \frac{\alpha}{2}\int_{\Omega} |\nabla z|^2 dxdy + \frac{\beta}{2}\int_{\Omega} \omega^P |z - f|^2 dxdy\right\}, \quad (8)$$

regularized and only the outline of the mark object remnant.

## 4 Mathematical Analysis

In this section, we will prove the convexity, existence, coercivity and uniqueness of the proposed functional Eq. (8).

**Convexity:** To prove that the model is convex, consider

$$E = |\nabla z| + \frac{\alpha}{2}|\nabla z|^2 + \frac{\alpha}{2}\omega^P|z - f|^2 \quad (10)$$

where $F = \int Edxdy$, and $F : \Omega \subset R2 \rightarrow R$

therefore,

$$E : \Omega \rightarrow R$$

Suppose that $P_1 = (x_1, y_1)$, $P_2 = (x_2, y_2)$ and for any $t \in [0,1]$, we have

$$tP_1 + (1-t)P_2 = t(x_1, y_1) + (1-t)(x_2, y_2) = t(x_1 - x_2) + x_2, t(y_1 - y_2) + y_2$$

Since $x_1, x_2 \in R$ so $x_1 - x_2 \in R$ and $t \in [0,1]$, this implies that, $t(x_1 - x_2) + x_2 \in R$ and $y_1 - y_2 \in R$ so, $(y_1 - y_2) + y_2 \in R$ and hence $tP_1 + (1-t)P_2 \in \Omega$ so the domain $\Omega$ is convex or in other words since $\Omega$ is a rectangle so it is convex. Now to check the convexity of $E$, we differentiate $E$ partially twice with respect to $z$ we get,

$$\frac{\partial E}{\partial z} = \beta\omega^P(z-f)$$

and

$$\frac{\partial^2 E}{\partial z^2} = \beta\omega^P$$

since $\beta$ is a positive constant and $\omega \in (0,1]$ so, $\frac{\partial^2 E}{\partial z^2} \geq 0$ and $\Omega$ is convex. Thus

$$E(tP_1 + (1-t)P_2) \leq tE(P_1) + (1-t)E(P_2)$$

holds for all $P_1, P_2 \in \Omega$ and $t \in [0,1]$. Now integrate $E$ we have,

$$\int E(tP_1 + (1-t)P_2)\,dxdy \leq t\int E(P_1)\,dxdy + (1-t)\int E(P_2)\,dxdy \quad (11)$$

$$F = \int Edxdy$$

so

$$F(tP_1 + (1-t)P_2) \leq tF(P_1) + (1-t)F(P_2). \quad (12)$$

Hence proved that $F$ is convex.

**Proposition 1.** If $f \in L^2(\Omega)$ and $\omega(x) > 0$. Then Eq. (8) is strictly convex and there exists a unique minimizer $z(x) \in W^{1,2}(\Omega)$.

**Proof: -** From the condition $\omega(x) > 0$ and Eq. (9) $\omega(x)$ is bounded.

Let $M_1 \leq \omega(x) \leq M_2$, where $M_1, M_2 > 0$.

Chose $z_0 = 0$, we have

$$0 \leq F(z) \leq F(z_0) = \frac{\beta}{2}\int_\Omega \omega^P f^2 dx \leq \frac{M_2^p\beta}{2}\|f\|^2_{L^2(\Omega)} < +\infty$$

Thus $F(z)$ must exist.

We now prove that $F(z)$ is coercive. It is clear that

$$\|\nabla z\|_{L^2(\Omega)} \leq \sqrt{\frac{2}{\alpha}F(z)} \quad (13)$$

also

$$\|z\|_{L^2(\Omega)} \leq \|z - f\|_{L^2(\Omega)}) + \|f\|_{L^2(\Omega)}. \quad (14)$$

Meanwhile,

$$0 \leq \frac{M_1^p\beta}{2}\int_\Omega |z-f|^2 dx \leq \frac{\beta}{2}\int_\Omega \omega^P|z-f|^2 dx \leq F(z).$$

From which we get,

$$\|z - f\|_{L^2(\Omega)}) \leq \sqrt{\frac{2}{M_1^p\beta}F(z)}\,. \quad (15)$$

Combining Eq. (13), (14) and (15) we have

$$\|z\|_{W^{1,2}(\Omega)} \leq \|z\|_{L^2(\Omega)} + \|\nabla z\|_{L^2(\Omega)} \leq \left(\sqrt{\frac{2}{\alpha}} + \sqrt{\frac{2}{M_1^p\beta}}\right)\sqrt{F(z)} + \|f\|_{L^2(\Omega)},$$

which means that $F(z)$ is coercive.

Note that $W^{1,2}(\Omega)$ is a reflective Banach space, and from Eq. (12) $F(z)$ is convex, lower semi continuous and coercive. We deduced that the minimizer of $F(z)$ will exist in $W^{1,2}(\Omega)$ [23, 45].

**Proposition 2.** Let $f \in L^2(\Omega)$ and $\omega(x) > 0$, then the unique minimizer $z^*(x)$ of Eq. (8) satisfies the inequality $inf_{x\in\Omega} f(x) \leq z^*(x) \leq sup_{x\in\Omega} f(x)$.

**Proof: -** It is obvious from proposition (1) that $F(z)$ is proper. Suppose that $z_n$ be a minimizing sequence. Then for $F(z_n)$ where $n \in N$ there exist a constant $M > 0$ such that $F(z_n) \leq M$. Therefore, $\|\nabla z_n\|_{L^2(\Omega)}$ are uniformly bounded. Moreover,

$$\frac{M_1^p\beta}{2}\|z_n - f\|^2_{L^2(\Omega)} \leq \frac{\beta}{2}\int_\Omega |z-f|^2 dx \leq M,$$

For all $n \in N$. From this we obtained that $\|z_n - f\|_{L^2(\Omega)}$ is uniformly bounded. Then we have,

$$\|z_n\|_{L^2(\Omega)} \leq \|z_n - f\|_{L^2(\Omega)} + \|f\|_{L^2(\Omega)}$$

is uniformly bounded.

Therefore, as a measure to $\nabla z^*$, $\nabla z_n$ converges weakly in $W^{1,2}(\Omega)$, and $z_n$ converges strongly to some $z^*$. Since $F(z)$ is lower semi-continuous, we Have

$$F(inf\ z_n) \leq inf\ F(z_n),$$

which implies that $z^*$ is the unique solution to Eq. (8).

Let $\alpha = inf\ f$ and $\beta = sup\ f$. We remark that $x \to \omega^p|x - f|2$ is decreasing in $(0, f)$ and increasing in $(f, +\infty)$. Therefore, if $C \geq f$, we have

$$\omega^p|min(x, C) - f|2 \leq \omega^p|x - f|2.$$

Let $C = \beta = sup\ f$, we get

$$\int_\Omega \omega^p|min(z^*, \beta) - f|2dx \leq \int_\Omega \omega^p|z^* - f|2dx \quad (16)$$

Similarly, we can prove that

$$\int_\Omega \omega^p|sup(z^*, \alpha) - f|2dx \leq \int_\Omega \omega^p|z^* - f|2dx \quad (17)$$

On the other hand, from G. David in [46], we have
and

$$sup(z^*,\alpha), min(z^*,\beta) \in W^{1,2}(\Omega)$$
$$|\nabla(min(z^*,\beta))| \leq |\nabla z^*|, \ |\nabla(sup(z^*,\alpha))| \leq |\nabla z^*|. \quad (18)$$

Combining (16), (17) and (18), we have

$$F(min(z^*,\beta)) \leq F(z^*), \ F(sup(z^*,\alpha)) \leq F(z^*)$$

which implies that $\alpha \leq z^* \leq \beta$.

## 5 Graphs Of Weight Function

In this section, we present some graphical analysis of the weight function defined in 9. In the Fig. 4 we present brain image in the first row and the graphs for $P = 2$, $P = 3$ and $P = 4$. From the Figures we can see that for the greater value of $P$ in the weight function the desired object segmented very well, and it's not captured the unwanted region. In the second row, we put an image of abdominal ultrasound and check the graph of the weight function for the different values of $P$ and it also shows that for the greater power of the weight function it gives the best result. In the figures, we also put some noisy images which are indicated by (i) and perform the experiment and conclude that the weight function performs well for the $P \geq 2$ and segment only the object of interest. The rectangle image is considered in the last row, and we give the graphical analysis of the segmentation result to use the new weight function. In the figures, (m) shows the given rectangle image and (n) presents the graph for $P = 2$ while the graph for $P = 3$ and $P = 4$ are given in the (o) and (p). For $P = 2$ in the weight function, the graph is not clear, and segmentation shows the unwanted region also with the desired object while for $P = 3$ and $P = 4$ it shows the best result.

## 6 Experiments

**Test Set-1**

In this subsection, we do some experiments on medical images and make comparisons with Mabood *et al.* [10] and Liu *et al.* [11] models in the Fig. 6. In the first row, (a) is the initial contour and (b) shows the performance of model [10] and in (c) we can see that model [10] which provide segmentation results but also captured the unwanted region. In the second row, (d) is the same initial contour and (e) shows the performance of model [11] and in (f) represent segmentation results of [11] which is also

**Test Set-4**

In this subsection, we accomplish experiments on an image of a rectangle and compare the segmented result of our model with Mabood *et al.* [10] and Liu *et al.* [11] models in Fig. 1. The first row shows the experimental result of [10], the second row shows the result of [11] while in the third row we consider our model and carry out the experiment to show the performance and segmented result of the new model. (a) is the initial contour in the first row (b) demonstrates the performance of model [10] and (c) shows the segmented result. (d) is the similar initial contour and (e) represent the

not efficient for of $P = 2$ in the weight function $\omega$. In the third row, we have considered the same initial contour as in (a) and (d) and perform the experiment, and (h) shows that the performance of the proposed model is better than the [10] and [11] models. In the last that in (i), we give the segmented result of our model, which captured only the object of interest as compared to the Mabood *et al.* and Liu *et al.* models.

**Test Set-2**

In this part, we exhibits experiments on some teeth infection images and analyze the segmented result of Mabood *et al.* [10] and Liu *et al.* [11] models with our model in the Fig. 7. In the first row, we present the exploratory outcome of [10], the second row shows the result of the model [11] and in the third row we examine our model and perform the experiment to present the achievement and the segmented result of the proposed model. The initial contour is shown in(a), (b) determine the performance of the model [10] and the segmented result presented in (c). In the second row of Fig. 7, we again consider the initial contour in (d) and did the experiment on Liu *et al.* model. The third row shows the achievement of our model. It is clear from this experiment that our model performs well.

**Test Set-3** In this section, we do experiments on an ultrasound image of the abdominal human body and compare the performance of our model with Mabood *et al.* [10] and Liu *et al.* [11] models in the Fig. 3. The figure consists of three rows, first row represents the experiment on the Mabood *et al.* model, the second row shows the achievement of Liu *et al.* model while in the third row we put our model performance. In the figure, (a), (d) and (g) is the given initial contour and the performance of model [10], [11] and our model are given in (b), (e) and (h) respectively. Segmented results are presented in (c), (f) and (i) of the model [10], [11] and our model respectively. By the comparisons, we conclude that the performance of our model is better than others.

achievement of model [11] and the segmented result of [11] are presented in (f). The third row of the Fig. 1 initial contour is indicated in (g) and (h) shows the performance of our model. From the performance and the segmented results given in Fig. 1, it is concluded that our model which is equipped with a new weight function performs better than the model [10] and that of the [11].

**a. Test Set-5**

Fig. 2 consists of three rows. In the first-row experimental result of Mabood *et al.* [10] model is given. In the second row, the performance, and the segmented result of Liu *et al.* [11] model is presented. The third row explores the achievement of the proposed model. (a), (d) and (g) are the same initial contour in the first, second and third rows respectively. the performances of the [10], [11] and the proposed model are identified by (b), (e) and (h) respectively. From the segmented results, we can see that the noisy synthetic image is not captured well by [10] and [11] models. And in the last row that is in (i), the appropriate segmented result is present which captured the circle or triangle. and this is the achievement of the proposed model.

**Test Set-6**

In this subsection, we equip experiments on an image of eye and make com- parisons with Mabood *et al.* [10] and Liu *et al.* [11] models in the Fig. 9. In the first row, (a) is the initial contour and the performance of model [10] given in (b) and in (c) we can see model [10] segmentation results but it is clear from the result that it is not performing better. In the second row,(d) is the same initial contour and (e) shows the performance of model [11] and the segmented result of model [11] is given in (f) which is also not efficient for of $P = 2$ in the weight function $\omega$. In the third row, we underestimate the same initial contour as in (a) and (d) and perform the experiment and it is shown that the performance of our model is better than the model [10] and model [11]. In the last that is in (i) we give the segmented result of the proposed model which captured the desired object well as compared to the Mabood *et al.* and Liu *et al.* models.

**Test Set-7**

We conduct experiments on an image of head fracture and make comparisons with [10] and [11] models in Fig. 5. In the first row, (a) indicate the initial contour and in (b) the performance of model [10] is given and the segmented result of [10] is shown in (c). From (c) the model segment the desired object but not properly. In the second row, we again perform the experiment on the same initial contour as in (a) which is represented by (d) the performance of model [11] is given in (e) while the segmented result of model [11] is shown in (f) which is better than [10] but it also segments some extra region which is not our desire. In the third row, we did the experiment on the initial contour as in (a) and (d) and it is shown that our model performs better than both models. In the last that is in (i) we give the segmented result of the new model which is equipped with a new weight function which gives better-segmented results of the desired object in the given image as compared to the Mabood *et al.* and Liu *et al.* models.

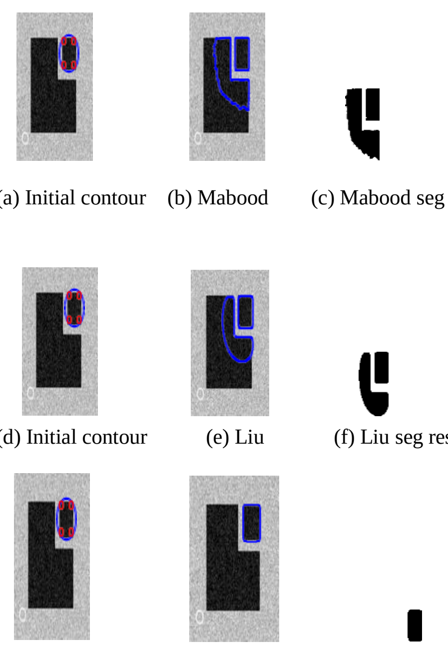

(a) Initial contour (b) Mabood (c) Mabood seg result

(d) Initial contour (e) Liu (f) Liu seg result

(g) Initial contour (h) Our (i) Our seg result

**Figure 1:** First row: Segmented result of Mabood *et al.* [10]. Second row: Segmented result of Liu *et al.* [11]. Third row: Segmented result of our proposed model for a noisy image. The performance of the proposed model is better than the others.

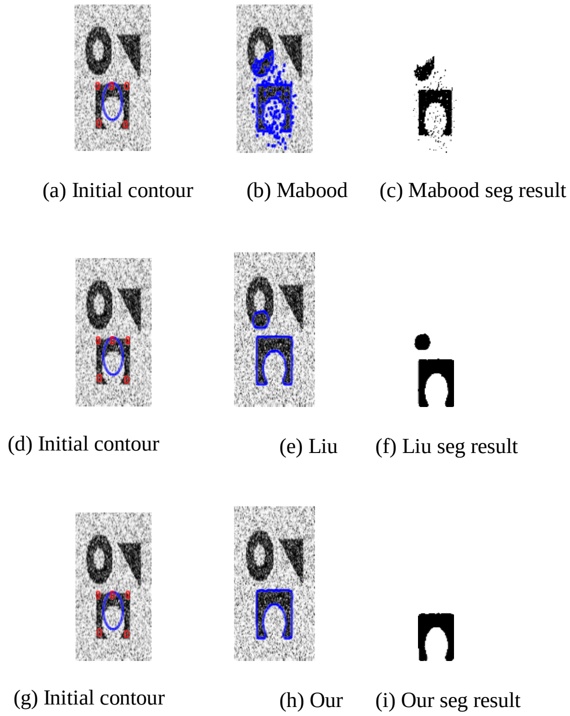

(a) Initial contour (b) Mabood (c) Mabood seg result

(d) Initial contour (e) Liu (f) Liu seg result

(g) Initial contour (h) Our (i) Our seg result

**Figure 2:** First row: Segmented result of Mabood *et al.* [10]. Second row: Segmented result of Liu *et al.* [11]. Third row: Segmented result of our model for a noisy image, it can be seen that our model successfully segments the region of interest.

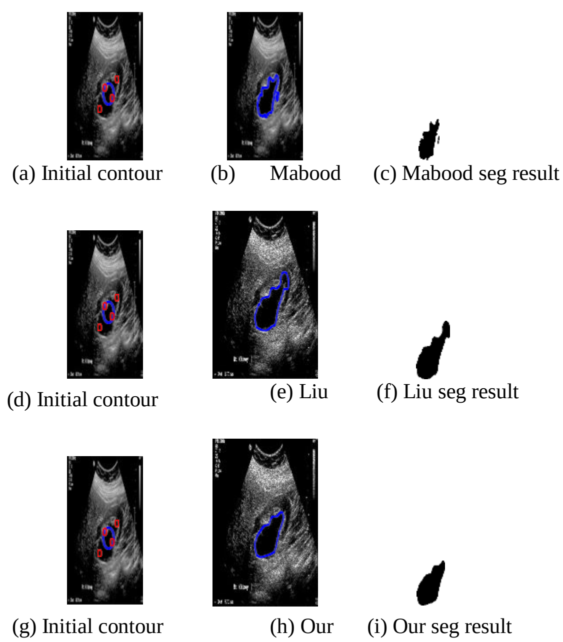

(a) Initial contour (b) Mabood (c) Mabood seg result

(d) Initial contour (e) Liu (f) Liu seg result

(g) Initial contour (h) Our (i) Our seg result

**Figure 3:** Segmenting image of ultrasound, First row: Segmented result of Mabood *et al.* [10]; Second row: Segmented result of Liu *et al.* [11]; Third row: Segmented result of our model. As compared to others the Proposed method successfully captured the region of interest.

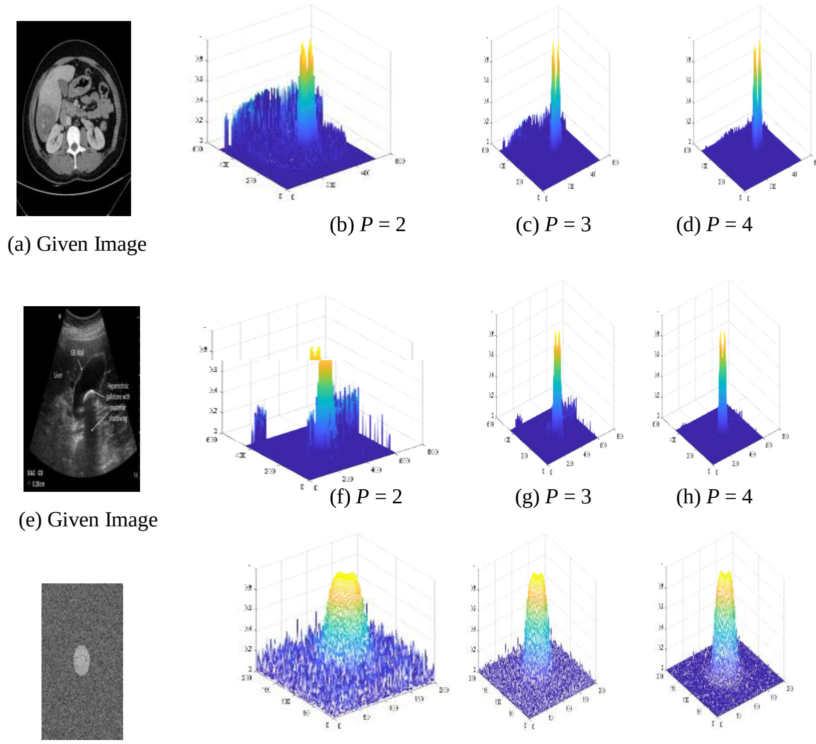

(a) Given Image (b) $P = 2$ (c) $P = 3$ (d) $P = 4$

(e) Given Image (f) $P = 2$ (g) $P = 3$ (h) $P = 4$

(i) Given Image (j) $P = 2$ (k) $P = 3$ (l) $P = 4$

**Figure 4:** 3-D Graph: Graphical analysis of new weight function on medical images and rectangle images showing the performance for $P = 2$, $P = 3$ and $P = 4$ in the weight function. For $P > 2$ the result is improved.

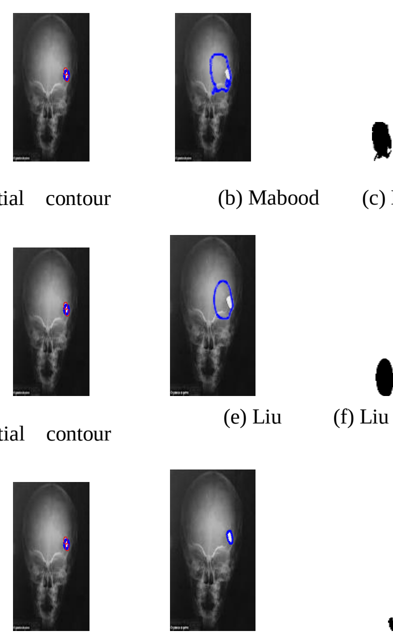

(a) Initial contour (b) Mabood (c) Mabood seg result

(d) Initial contour (e) Liu (f) Liu seg result

(g) Initial contour (h) Our (i) Our seg result

**Figure 5:** Comparison of Mabood *et al.* [10], Liu *et al.* [11] and our model on segmenting a head fracture image. The proposed model successfully detected the object of interest as compared to [10] and [11].

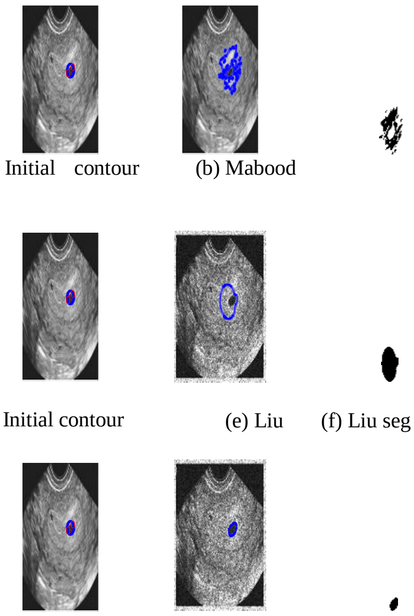

(a) Initial contour (b) Mabood (c) Mabood seg result

(d) Initial contour (e) Liu (f) Liu seg result

(g) Initial contour (h) Our (i) Our seg result

**Figure 6**: Segmenting an abdominal ultrasound image, First row: Segmented result of Mabood *et al.* [10]. Second row: Segmented result of Liu *et al.* [11]. Third row: Segmented result of our model.

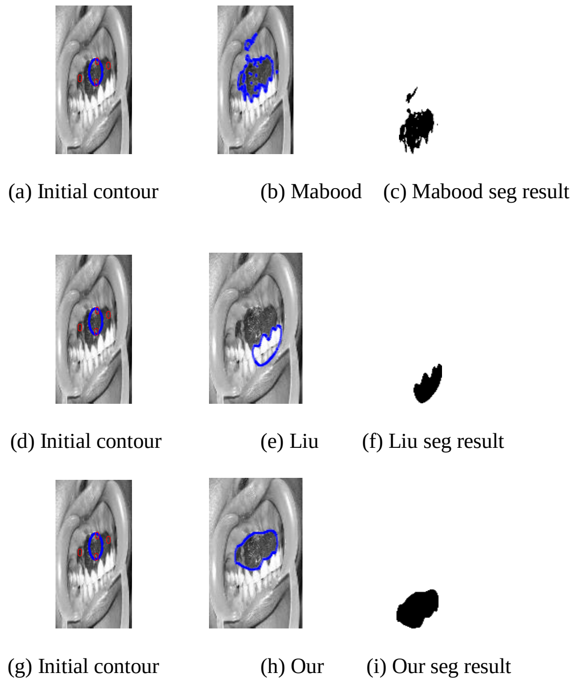


**Figure 7:** Segmenting an infected Gingiva image, First row: Segmented result of Mabood *et al*. [10]. Second row: Segmented results of Liu *et al.* [11]. Third row: Segmented results of the proposed model.

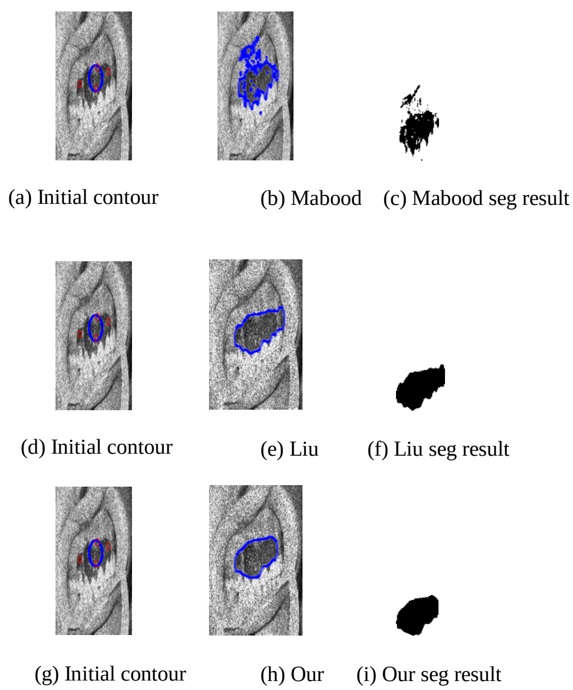


**Figure 8**: First row: Segmented result of Mabood *et al.* [10]. Second row: Segmented result of Liu *et al.* [11]. Third row: Segmented result of our model.

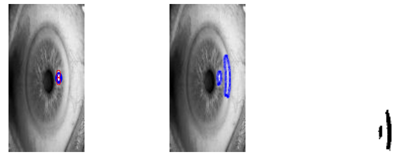

(a) Initial contour (b) Mabood (c) Mabood seg result

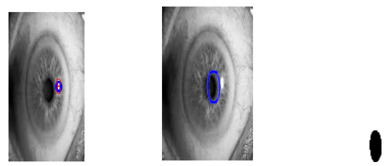

(d) Initial contour (e) Liu (f) Liu seg result

(g) Initial contour (h) Our (i) Our seg result

**Figure 9**: First row: Segmented result of Mabood *et al.* [10]. Second row: Performance of Liu *et al.* [11]. Third row: Result shows the performance of the proposed model.

**Acknowledgement**

The authors would like to thank the anonymous reviewers for their valuables suggestions that helped improve the presentation of this paper. The code of the proposed method will be provided for research purposes if requested via email.

## 7 Conclusion

In this paper, we proposed a convex selective segmentation model based on the Mumford-Shah model and perform segmentation in two stages. To ad- just the fidelity and smoothing terms, a weight function is incorporated for selecting some marker points around the edge of the object in each image. For the smooth solution, we solve the model by using ADM, which preserves the main structure of the target and filters out the details far away from the edge. Then by thresholding, the segmentation can be obtained. Experimental results on medical and noisy images show the robustness, efficiency, and effectiveness of the proposed method.

## References

[1] Mumford, D. B., Shah, J. (1989). Optimal approximations by piecewise smooth functions and associated variational problems. Communications on pure and applied mathematics.

[2] Kass, M., Witkin, A., Terzopoulos, D. (1988). Snakes: Active contour models. Int. J. Comput. Vis, 1(4), 321-331.

[3] Caselles, V., Kimmel, R., Sapiro, G. (1997). Geodesic active contours. Int. J. Comput. Vis, 22, 61-79.

[4] Xiang, Y., Chung, A.C.S., Ye, J. (2006). An active contour model for image segmentation based on elastic interaction. J. Comput. Phys, 219, 455-476.

[5] Gout, C., Le Guyader, C., Vese, L. (2005). Segmentation under geo- metrical conditions with geodesic active contour and interpolation using level set methods. Numer. Algorithms, 39, 155-173.

[6] Badshah, N., Chen, K. (2009). Image selective segmentation under geometry constrains using an active contour approach. Communications in Computational Physics, 7(4), 759.

[7] Zhang, J., Chen, K., Yu, B., Gould, D. A. (2014). A local information based variational model for selective image segmentation. Inverse Problems. Imaging, 8(1), 293.

[8] Rada, L., Chen, K. (2012). A new variational model with dual level set functions for selective segmentation. Commun. Comput. Phys, 12, 261-283.

[9] Peng, J., Dong, F., Chen, Y., Kong, D. (2014). A region-appearance- based adaptive variational model for 3D liver segmentation. Med. phys, 41(4), 043502.

[10] Mabood, L., Ali, H., Badshah, N., Chen, K., Khan, G. A. (2016). Active contours textural and inhomogeneous object extraction. Pattern Recognition, 55, 87-99.

[11] Liu, C., Ng, M. K. P., Zeng, T. (2018). Weighted Variational Model for Selective Image Segmentation with Application to Medical Images. Pattern Recognition, 76, 367-379.

[12] Osher, S., Sethian, J.A. (1988). Fronts propagating with curvature-dependent speed: algorithms based on Hamilton-Jacobi formulations.

J. Comput. Phys, 79, 12-49.

[13] Chan, T.F., Vese, L.A. (2001). Active contour without edges. IEEE Trans. Image Process, 10, 266-277.

[14] Vese, L.A., Chan, T.F. (2002). A multiphase level set framework for image segmentation using the Mumford and Shah model. Int. J. Comput. Vis, 50, 271-293.

[15] Lie, J., Lysaker, M., Tai, X. C. (2006). A variant of the level set method and applications to image segmentation. Math. Comput, 75, 11551174.

[16] Zhu, S., Wu, Q., Liu, C. (2011). Shape and topology optimization for elliptic boundary value problems using a piecewise constant level set method. Appl. Numer. Math, 61, 752-767.

[17] Zhu, S., Liu, C., Wu, Q. (2010). Binary level set methods for topology and shape optimization of a two-density inhomogeneous drum. Comput. Methods Appl. Mech. Engrg, 199, 2970-2986.

[18] Li, F., Ng, M., Zeng, T., Shen, C. (2010). A multiphase image segmentation method based on fuzzy region competition. SIAM J. Imaging Sci, 3, 277-299.

[19] Mory, B., Ardon, R. (2007). Fuzzy region competition: a convex two- phase segmentation framework. in: Scale Space and Variational Methods in Computer Vision, 214-226.

[20] Grady, L., Alvino, C. (2008). Reformulating and optimizing the Mumford-Shah functional on a graph- A faster, lower energy solution. in: Proceedings of the European Conference on Computer Vision (ECCV), 248-261.

[21] Chan, T.F., Esedoglu, S., Nikolova, M. (2006). Algorithms for finding global minimizers of image segmentation and denoising models. SIAM J. Appl. Math, 66, 1632-1648.

[22] Pock, T., Chambolle, A., Cremers, D., Bischof, H. (2009). A convex relaxation approach for computing minimal partition. in: Proceedings of the IEEE Computer Society Conference on Computer Vision and Pattern Recognition (CVPR), 810-817.

[23] Cai, X., Chan, R., Zeng, T. (2013). A two-stage image segmentation method using a convex variant of the Mumford-Shah model and thresholding. SIAM J. Imaging Sci, 6, 368-390.

[24] Goldstein, T., Osher, S. (2009). The split Bregman method for L1-regularized problems. SIAM J. Imaging Sci, 2, 323-343.

[25] Zhang, X., Burger, M., Osher, S. (2011). A united primal-dual algorithm framework based on Bregman iteration. J. Sci. Comput, 46, 20-46.

[26] Cai, X. (2015). Variational image segmentation model coupled with image restoration achievements. Pattern Recogn, 48, 2029-2042.

[27] Awate, S.P., Whitaker, R.T. (2014). Multiatlas segmentation as non- parametric regression. IEEE Trans. Med. Imaging, 33, 1803-1817.

[28] Dam, E.B., Lillhol, M., Marques, J., Nielsen, M. (2015). Automatic segmentation of high-and low field knee MRIs using knee image quantification with data from the osteoarthritis initiative. J. Med. Imaging, 2, 024001.

[29] Awate, S.P., Tasdizen, T., Whitaker, R.T. (2006). Unsupervised texture segmentation with nonparametric neighborhood statistics. European Conference on Computer Vision, 494-507.

[30] Kim, J., Yezzi, A., Cetin, M., Willsky, A.S. (2005). A

nonparametric statistical method for image segmentation using information theory and curve evolution. IEEE Trans. Image Process, 14, 1486-1502.

[31] Liu, J., Zhang, X., Dong, B., Shen, Z., Gu, L. (2015). A wavelet frame method with shape prior for ultrasound video segmentation. SIAM J. Imaging Sci, 9, 495-519.

[32] Hui, Z., Trevor, H. (2005). Regularization and variable selection via elastic net. J. R. Statist. Soc. B, 67, 301-320.

[33] Chambolle, A. (1995). Image segmentation by variational methods: Mumford and Shah functional and the discrete approximations. SIAM J. Appl. Math, 55, 827-863.

[34] Liu, C., Dong, F., Zhu, S., Kong, D., Liu, K. (2011). New variational formulations for level set evolution without reinitialization with applications to image segmentation. J. Math. Imaging Vis, 41, 194-209.

[35] Esedoglu, S., Tsai, Y. (2006). Threshold dynamics for the piecewise constant Mumford-Shah functional. J. Comput. Phys, 211, 367-384.

[36] Zhao, Y., Rada, L., Chen, K., Simon, Harding, P., Zheng, Y. (2015). Automated vessel segmentation using infinite perimeter active contour model with hybrid region information with application to retinal images. IEEE Trans. Med. Imaging, 34, 1797-1807.

[37] Limberger, F.A., Oliveira, M.M. (2015). Real-time detection of planar regions in unorganized point clouds. Pattern Recogn, 48, 2043-2053.

[38] Min, H., Jia, W., Wang, X.F., Zhao, Y., Hu, R.X., Luo, Y.T., Xue, F., Lu, J.T. (2015). An Intensity-Texture model-based level set method for image segmentation Pattern Recogn, 48, 1547-1562.

[39] Ji, H.K., Sun, Q.S., Ji, Z.X., Yuan, Y.H., Zhang, G.Q. (2016). Collaborative probabilistic labels for face recognition from single sample per person. Pattern Recogn, 62, 125-134.

[40] Cai, X. (2015). Variational image segmentation model coupled with image restoration achievements. Pattern Recogn, 48, 2029-2042.

[41] Hartigan, J., Wang, M. (1979). A K-means clustering algorithm. Algorithm AS 136, Appl. Statist, 28, 100-108.

[42] Lindsten, F., Ohlsson, H., Ljung, L. (2011). Just relax and come clustering! A convexification of k-means clustering. Technical Report 2992, Linkping University.

[43] Nguyen, T., Cai, J., Zhang, J., Zheng, J. (2012). Robust interactive image segmentation using convex active contours. IEEE Trans. Image Process, 21, 3734-3743.

[44] Liu, C., K-Po Ng, M., Zeng, T. (2017). Weighted Variational Model for Selective Image Segmentation with Application to Medical Images.

Pattern Recognition. doi: 10.1016/j.patcog.2017.11.019

[45] Ekeland, I., Temam, R. (1999) Convex Analysis and Variational Problems. Classics in Appl. Math, 28, SIAM.

[46] David, G. (2006). Singular Sets of Minimizers for the Mumford-Shah Functional. Springer Science & Business Media. Vol. 233.